Models for turbulent plane Couette flow using the proper orthogonal decomposition

J. Moehlis
Program in Applied and Computational Mathematics, Princeton University, Princeton, New Jersey 08544

T. R. Smith
Department of Mechanical and Aerospace Engineering, Princeton University, Princeton, New Jersey 08544

P. Holmes[a)]
*Program in Applied and Computational Mathematics, Princeton University, Princeton, New Jersey 08544
and Department of Mechanical and Aerospace Engineering, Princeton University, Princeton,
New Jersey 08544*

H. Faisst
Fachbereich Physik, Philipps Universität Marburg, D-35032 Marburg, Germany

We model turbulent plane Couette flow (PCF) by expanding the velocity field as a sum of optimal modes calculated via the proper orthogonal decomposition from numerical data. Ordinary differential equations are obtained by Galerkin projection of the Navier–Stokes equations onto these modes. For a minimal truncation including only the most energetic modes having no streamwise variation, we show under quite general conditions the existence of linearly stable nontrivial fixed points, corresponding to a state in which the mean flow is coupled to streamwise vortices and their associated streaks. When the two next most energetic modes, still lacking streamwise variations, are included, chaos and heteroclinic cycles associated with the fixed points are found. The attractors involve repeated visits near unstable fixed points and periodic orbits corresponding to steady and periodically varying vortices, and account for a self-sustaining process in which vortices interact with the mean flow. The models considered in this paper can also serve as a foundation for more sophisticated ordinary differential equation models for turbulent PCF, including those which include modes with streamwise variations. © *2002 American Institute of Physics.*
[DOI: 10.1063/1.1483300]

I. INTRODUCTION

In 1967, Lumley[1] (cf. Ref. 2) suggested that the proper orthogonal decomposition (POD) could be used to extract energetic, and hence presumably dynamically relevant, coherent structures from turbulent velocity fields. However, the two-point velocity correlation tensors required for the derivation of the empirical basis functions of the POD demand the collection of large amounts of data, and not until the 1980's did experimental and computational techniques develop to the point at which this remarkable idea could flourish. Working with hot film anemometry, Herzog[3] provided turbulent boundary layer data which Aubry *et al.*[4] (hereafter AHLS) used to create a low-dimensional model of the wall region by projection of the Navier–Stokes equations (NSE) onto empirical subspaces, following modeling of the mean (spatially averaged) flow and use of a Heisenberg-type model to account for energy transfer to neglected modes. This model captured aspects of the experimentally observed ejection and bursting events associated with streamwise vortex

pairs.[5] AHLS, and parallel work of Sirovich,[6] led to a number of similar studies; see Ref. 7 for background and further citations.

In this paper, we consider a simpler problem than the fully developed turbulent boundary layer: Plane Couette flow (PCF) at a relatively modest Reynolds number. PCF has many interesting properties, including: (i) linear stability of the laminar state for all Reynolds numbers Re,[8] (ii) the experimental observation of turbulence for sufficiently high Re and/or perturbation amplitudes,[9] and (iii) the existence of unstable finite amplitude solutions consisting of streamwise vortices and streaks which do not bifurcate from the laminar state.[10–12] While progress in understanding these and other properties of PCF turbulence has been made through experiments and the numerical study of the NSE, ordinary differential equation (ODE) models have provided additional insight. For example, the models reviewed in Ref. 13 emphasize non-normality of the linearized Navier–Stokes operator, proposing that the resulting transient growth of perturbations may trigger a nonlinear transition to turbulence. Weaknesses of such models are that they are not derived in a systematic way from the NSE, and in fact often violate basic nonlinear properties of the NSE.[14] The model considered in Refs. 15 and 16 (following previous work in Refs. 14, 17,

---
[a)]Author to whom correspondence should be addressed. Telephone: 609-258-2958; fax: 609-258-6109; electronic mail: pholmes@rimbaud.princeton.edu

and 18) views the turbulent state as being related to a nonlinear "self-sustaining process" involving streamwise rolls, streaks and their instabilities, all feeding off the mean flow; see also Ref. 19. Stable fixed points or periodic orbits for the model are associated with the turbulent state. A related higher-dimensional model[12,20] captures the existence of many unstable finite amplitude solutions, and suggests that the transition boundary is characterized by a chaotic repeller.[21] Note that the models in Refs. 12, 15, 16, and 20 are for sinusoidal shear flow, which is related to but not identical to PCF.

While these ODE models successfully capture various aspects of the PCF system, the description of the sustained turbulent state as a fixed point (corresponding to steady fluid flow) or a periodic orbit (corresponding to periodic fluid flow) is undoubtedly too simple. In this paper, we use the approach described in AHLS to suggest a more sophisticated characterization of the sustained turbulent state. In particular, we investigate in detail the interesting possibility, suggested for PCF in Refs. 12 and 22 and partially demonstrated for the turbulent boundary layer in AHLS and Refs. 23, 24, that fully developed PCF turbulence might be related to heteroclinic connections among unstable, ordered structures in the flow, such as streamwise vortices. This nicely resolves the paradox that streamwise vortices are observed "on average," and hence are represented among the leading empirical eigenfunctions, both in the boundary layer[4,7] and in the present study, even though they are ostensibly linearly unstable due to the inflection-point shear profiles they induce. Repeated visits to the neighborhoods of unstable sets are a necessary consequence of heteroclinic cycles.

Specifically, using well-resolved data for the turbulent state obtained from numerical simulations, we perform a POD which identifies an energetically dominant set of empirical eigenmodes ("POD modes") from the data. We then construct models by Galerkin projection of the NSE onto finite-dimensional subspaces spanned by the dominant modes; this yields ODEs for the evolution of the modal amplitudes. After verifying the validity of this procedure by examining truncations which retain a large number of terms, we consider low-dimensional models; because the modes optimally represent the cumulative kinetic energy, it is hoped that these low-dimensional models will capture important aspects of the turbulence. In studying the low-dimensional models, we pay particular attention to symmetries of the PCF system and their implications for the ODEs. Our analysis suggests that heteroclinic cycles and chaos are important correlates of sustained turbulence. Note that the model in Refs. 12, 15, 16, and 20 are also obtained through Galerkin projection of the NSE, but they use elementary (and nonoptimal) trigonometric bases.

As in AHLS, the modes included in the present study lack streamwise structure. While this is clearly restrictive, we believe that it is a useful starting point for understanding models which include streamwise variations. (For example, Sec. IV of Hamilton *et al.*[17] uses "zeroed" streamwise modes to investigate the effect of vortices on the turbulent mean.) Moreover, there are important differences between the present models and those considered in AHLS. First, the present models apply to the *entire* channel and thus not only describe boundary layer dynamics, but also include modal interactions characteristic of the full channel. Moreover, inclusion of the entire domain eliminates the pressure forcing term required in AHLS. (Zhou and Sirovich[25,26] also used full channel POD modes, but with a wall-weighted norm, to extract a boundary layer model, cf. Ref. 7, Sec. 11.5.) Second, PCF has an *exact* laminar solution, whose (constant) shear can act as an energy source for turbulence. We allow the mean of perturbations to this laminar solution to evolve under the NSE rather than modeling the turbulent mean as in AHLS. Finally, the governing equations for PCF enjoy more spatial symmetry than those for the turbulent boundary layer. These symmetries, plus the fact that the nonlinear terms conserve energy, constrain the projected ODEs, permitting checks to be performed on the resulting models, and simplifying their analysis.

In applying the POD and projection method to one of the simplest nontrivial shear flows, we hope to provide a critical assessment of the method by making direct comparisons of model predictions with direct numerical simulation (DNS) and experimental results. In this first paper we confirm that relatively high $[\mathcal{O}(600\text{-}1200)\text{-}]$ dimensional projections can capture the observed modal energy budgets and provide acceptable short-term tracking of individual solutions, and we show that very low $[\mathcal{O}(2\text{-}10)\text{-}]$ dimensional models can reveal qualitative mechanisms by which low Reynolds number turbulence is sustained and cross stream length scales are selected. We find that the detailed behavior depends in a subtle manner on the modes included in the truncation, and that a proper account of the symmetries of the system is crucial.

We begin by giving the governing equations for PCF and discussing their symmetries in Sec. II. Sec. III describes the POD modes derived from turbulent PCF data. In Sec. IV, after verifying that high-dimensional models of turbulent PCF derived using the POD and Galerkin projection of the NSE can accurately reproduce the flow properties, we describe results for two different classes of low-dimensional models. We summarize our results in Sec. V.

II. PLANE COUETTE FLOW: EQUATIONS AND SYMMETRIES

In PCF, fluid is sheared between two infinite parallel plates moving at speed U_0, in opposite directions $\pm \mathbf{e}_x$. The x, y, z directions are defined to be the streamwise, spanwise, and wall normal directions, respectively. We nondimensionalize lengths in units of $d/2$ where d is the gap between the plates, velocities in units of U_0, time in units of $(d/2)/U_0$, and pressure in units of $U_0^2 \rho$ where ρ is the fluid density. Laminar flow is then given by $\mathbf{U}_0 = z\mathbf{e}_x$, $-1 \leq z \leq 1$. Writing $\mathbf{u} = (u_1, u_2, u_3)$, $\mathbf{x} = (x, y, z)$, the evolution equation for the perturbation $[\mathbf{u}(\mathbf{x}, t), p(\mathbf{x}, t)]$ to laminar flow is

$$\frac{\partial}{\partial t}\mathbf{u} = -(\mathbf{u} \cdot \nabla)\mathbf{u} - z\frac{\partial}{\partial x}\mathbf{u} - u_3\mathbf{e}_x - \nabla p + \frac{1}{Re}\nabla^2 \mathbf{u}, \quad (1)$$

where the Reynolds number Re is defined by

$$Re = \frac{U_0 d}{2\nu}. \tag{2}$$

The fluid is assumed to be incompressible, i.e.,

$$\nabla \cdot \mathbf{u} = 0, \tag{3}$$

and there are no-slip boundary conditions at the plates, i.e.,

$$\mathbf{u}|_{z=\pm 1} = 0. \tag{4}$$

Finally, the flow is assumed periodic in the streamwise and spanwise directions, with lengths $L_x \equiv 4\pi$ and $L_y \equiv 2\pi$, respectively, following Refs. 10–12. We denote the domain $0 \leq x \leq L_x$, $0 \leq y \leq L_y$, $-1 \leq z \leq 1$ by Ω.

Equations (1) and (3) along with the boundary conditions are equivariant with respect to the following symmetries[12]

$$\mathcal{P} \cdot [(u_1, u_2, u_3, p)(x, y, z, t)]$$
$$= (-u_1, -u_2, -u_3, p)(-x, -y, -z, t), \tag{5}$$

$$\mathcal{R} \cdot [(u_1, u_2, u_3, p)(x, y, z, t)]$$
$$= (u_1, -u_2, u_3, p)(x, -y, z, t), \tag{6}$$

$$\mathcal{R}\mathcal{P} \cdot [(u_1, u_2, u_3, p)(x, y, z, t)]$$
$$= (-u_1, u_2, -u_3, p)(-x, y, -z, t), \tag{7}$$

$$\mathcal{T}_{\Delta x, \Delta y} \cdot [(u_1, u_2, u_3, p)(x, y, z, t)]$$
$$= (u_1, u_2, u_3, p)(x + \Delta x, y + \Delta y, z, t). \tag{8}$$

Equivariance means that if there is a solution $\mathbf{u}(\mathbf{x}, t)$ to (1), then the solution obtained by acting on $\mathbf{u}(\mathbf{x}, t)$ with any product of the actions given in Eqs. (5)–(8) will also be a solution. For example, if

$$(u_1(x, y, z, t), u_2(x, y, z, t), u_3(x, y, z, t), p(x, y, z, t))$$

solves (1), then so does

$$(u_1(x, -y, z, t), -u_2(x, -y, z, t),$$
$$u_3(x, -y, z, t), p(x, -y, z, t)).$$

Physically, $\mathcal{P}$ is a point reflection about $(x, y, z) = (0, 0, 0)$, $\mathcal{R}$ is a reflection about the plane $y = 0$, $\mathcal{R}\mathcal{P}$ is a rotation by π about the y axis, and $\mathcal{T}_{\Delta x, \Delta y}$ is a translation by Δx in the streamwise direction and by Δy in the spanwise direction. $\mathcal{P}$ and $\mathcal{R}$ generate the four element group $\{\mathrm{Id}, \mathcal{P}, \mathcal{R}, \mathcal{R}\mathcal{P}\}$, isomorphic to the abstract group D_2 (see, e.g., Ref. 27). The group generated by $\mathcal{R}\mathcal{P}$ and translations in the x direction is $O(2) = Z_2(\mathcal{R}\mathcal{P}) \ltimes S^1(\mathcal{T}_{\Delta x})$ where $\ltimes$ denotes the semidirect product, and the group generated by $\mathcal{R}$ and translations in the y direction is $O(2) = Z_2(\mathcal{R}) \ltimes S^1(\mathcal{T}_{\Delta y})$. Altogether, the governing equations are equivariant with respect to the direct product of these groups, i.e., $O(2) \times O(2)$. We note that the boundary layer of AHLS shares only *some* of the symmetries of the PCF system: It lacks $\mathcal{P}$ and $\mathcal{P}\mathcal{R}$ and altogether has $O(2) \times S^1$ symmetry, where $O(2) = Z_2(\mathcal{P}) \ltimes S^1(\mathcal{T}_{\Delta y})$ and $S^1 = S^1(\mathcal{T}_{\Delta x})$. We will use the symmetries in our application of the POD procedure to create a basis endowed with the appropriate symmetries.

III. POD MODES FOR PLANE COUETTE FLOW

A. The POD procedure

Details of the POD procedure are described in Ref. 7; here we summarize key aspects. The POD modes $\Phi = (\Phi_1, \Phi_2, \Phi_3)$ are chosen to maximize the average projection of the perturbation $\mathbf{u} = (u_1, u_2, u_3)$ onto each mode. First, we define the inner product on the space of velocity fields $[L^2(\Omega)]^3$ as

$$(\mathbf{f}, \mathbf{g}) \equiv \sum_{j=1}^{3} \int \int \int_{\Omega} f_j(\mathbf{x}) g_j^*(\mathbf{x}) d^3\mathbf{x},$$

where the subscripts identify components of the functions and * denotes complex conjugation. The POD modes are chosen to maximize the average projection of the perturbation $\mathbf{u}$ onto each mode; specifically, we seek functions $\Phi(\mathbf{x}) \in [L^2(\Omega)]^3$ such that the quantity $\langle |(\mathbf{u}, \Phi)|^2 \rangle / \|\Phi\|^2$ is maximized, where $\| \cdot \| = (\cdot, \cdot)^{1/2}$ and $\langle \cdot \rangle$ is an (ensemble or time) averaging operation. This leads to the eigenvalue problem

$$\sum_{j=1}^{3} \int \int \int_{\Omega} \langle u_i(\mathbf{x}, t) u_j^*(\mathbf{x}', t) \rangle \Phi_{jn_x n_y}^{(n)}(\mathbf{x}') d^3\mathbf{x}'$$
$$= \lambda_{n_x n_y}^{(n)} \Phi_{in_x n_y}^{(n)}(\mathbf{x}), \quad i = 1, 2, 3, \tag{9}$$

where the "quantum numbers" $n \in Z^+$, and wave numbers $n_x, n_y \in Z$ distinguish different POD modes. The eigenvalue $\lambda_{n_x n_y}^{(n)}$ is twice the average kinetic energy in the POD mode $\Phi_{n_x n_y}^{(n)}$ [see (14) below]. The (orthogonal) POD modes will be normalized so that

$$(\Phi_{n_x n_y}^{(n)}, \Phi_{n_x' n_y'}^{(n')}) = \delta_{nn'} \delta_{n_x n_x'} \delta_{n_y n_y'}.$$

The POD modes are optimal in the sense of capturing, on average, the most kinetic energy possible for a projection onto a given number of modes. In applications one is typically only interested in POD modes $\Phi_{n_x n_y}^{(n)}$ with strictly positive eigenvalues $\lambda_{n_x n_y}^{(n)}$. While these do not form a complete basis, almost every member of the original ensemble used to obtain the POD modes can be reproduced by linear combinations of the POD modes; moreover each $\Phi_{n_x n_y}^{(n)}$ inherits linear properties from the ensemble $\{\mathbf{u}^{(k)}\}$, such as incompressibility and boundary conditions. Finally, we note that the POD procedure can be formulated for other inner products (e.g., Ref. 28), allowing the computation of POD modes which optimally represent quantities other than the kinetic energy.

B. Application to plane Couette flow

We expand the perturbation velocity field $\mathbf{u}$ in terms of POD modes as

$$\mathbf{u}(\mathbf{x}, t) = \sum_{n=1}^{\infty} \sum_{n_x = -\infty}^{\infty} \sum_{n_y = -\infty}^{\infty} a_{n_x n_y}^{(n)}(t) \Phi_{n_x n_y}^{(n)}(\mathbf{x}), \tag{10}$$

where the amplitudes $a_{n_x n_y}^{(n)}$ are complex unless $n_x = n_y = 0$, in which case they are real. Note that the vector-valued functions $\Phi_{n_x n_y}^{(n)}$ effectively couple all three components of the

velocity field; this has implications to which we shall return. Translation symmetry in x and y implies optimality of the Fourier decomposition in these directions[7]

$$\Phi_{n_x n_y}^{(n)}(\mathbf{x}) = \frac{\phi_{n_x n_y}^{(n)}(z)}{\sqrt{L_x L_y}} \exp\left(2\pi i \left(\frac{n_x x}{L_x} + \frac{n_y y}{L_y} \right) \right). \tag{11}$$

Complex conjugating (9) and using (11) gives

$$\phi_{n_x n_y}^{(n)}(z) = \phi_{-n_x -n_y}^{(n)*}(z). \tag{12}$$

Since $\mathbf{u}$ is real, (10) then implies that

$$a_{n_x n_y}^{(n)}(t) = a_{-n_x -n_y}^{(n)*}(t). \tag{13}$$

We also note that[7]

$$\lambda_{n_x n_y}^{(n)} = \langle |a_{n_x n_y}^{(n)}|^2 \rangle \quad \text{and} \quad \langle a_{n_x n_y}^{(n)} a_{k_x k_y}^{(k)*} \rangle = 0,$$

$$\text{unless} \quad k = n, k_x = n_x, k_y = n_y. \tag{14}$$

The DNS velocity data is computed in the form

$$\mathbf{u}(\mathbf{x},t) = \sum_{n_x n_y} \exp\left(2\pi i \left(\frac{n_x x}{L_x} + \frac{n_y y}{L_y} \right) \right) \mathbf{F}(n_x, n_y; z, t), \tag{15}$$

and reality of $\mathbf{u}$ implies that

$$\mathbf{F}(-n_x, -n_y; z, t) = \mathbf{F}^*(n_x, n_y; z, t). \tag{16}$$

Substituting Eqs. (15) and (11) into (9), integrating over x' and y', and Fourier transforming in x and y, we obtain

$$L_x L_y \sum_{j=1}^{3} \int_{-1}^{1} \langle F_i(n_x, n_y; z, t) F_j^*(n_x, n_y; z', t) \rangle$$

$$\times \phi_{j n_x n_y}^{(n)}(z') dz' = \lambda_{n_x n_y}^{(n)} \phi_{i n_x n_y}^{(n)}(z). \tag{17}$$

We now consider computation of the kernel $\langle F_i F_j^* \rangle$ of (17). The data are not given for continuous t, but rather as a series of *snapshots* at discrete times t_k

$$\mathbf{u}^{(k)}(\mathbf{x}) = \sum_{n_x n_y} \exp\left(2\pi i \left(\frac{n_x x}{L_x} + \frac{n_y y}{L_y} \right) \right) \mathbf{F}^{(k)}(n_x, n_y; z), \tag{18}$$

where $\mathbf{u}^{(k)}$ is the kth snapshot of $\mathbf{u}$, and $\mathbf{F}^{(k)}$ is the corresponding kth snapshot of $\mathbf{F}$. One might be tempted to take

$$\langle F_i(n_x, n_y; z, t) F_j^*(n_x, n_y; z', t) \rangle$$

$$= \frac{1}{T'} \sum_{k=1}^{T'} F_i^{(k)}(n_x, n_y; z) F_j^{(k)*}(n_x, n_y; z'), \tag{19}$$

where T' is the number of snapshots in the original ensemble. However, it has been pointed out[6] that the symmetries of such systems can be used to enlarge the ensemble size without having to solve the governing equations for new initial conditions, and it was subsequently noted that, to obtain bases which appropriately retain all symmetries of the governing equations, it is in fact *necessary* to average over orbits of the symmetry group.[29–32] For the present system, translation symmetries in the streamwise and spanwise direc-

tion are accounted for by the Fourier decomposition (11). The kernel obtained by averaging over the remaining symmetry group $D_2 = \{\text{Id}, \mathcal{P}, \mathcal{R}, \mathcal{R}\mathcal{P}\}$ is given by

$$\langle F_i(n_x, n_y; z, t) F_j^*(n_x, n_y; z', t) \rangle$$

$$= \frac{1}{T'} \sum_{l=1}^{T'} \sum_{\gamma \in D_2} \gamma \cdot F_i^{(l)}(n_x, n_y; z)$$

$$\times \gamma \cdot F_j^{(k)*}(n_x, n_y; z')$$

$$\equiv \frac{1}{T} \sum_{k=1}^{T} F_i^{(k)}(n_x, n_y; z) F_j^{(k)*}(n_x, n_y; z'), \tag{20}$$

where the set of snapshots is extended in the obvious way to give a total of $T = 4T'$ velocity fields. The actions of the elements of D_2 on the $\mathbf{F}^{(k)}$'s are given in Appendix A. Equation (17) thus becomes

$$\frac{L_x L_y}{T} \sum_{j=1}^{3} \int_{-1}^{1} \sum_{k=1}^{T} F_i^{(k)}(n_x, n_y; z) F_j^{(k)*}(n_x, n_y; z')$$

$$\times \phi_{j n_x n_y}^{(n)}(z') dz' = \lambda_{n_x n_y}^{(n)} \phi_{i n_x n_y}^{(n)}(z). \tag{21}$$

Numerical methods are used to solve (21) for the ϕ's, represented as vectors specifying values at discrete spatial locations. This can be accomplished by the method of snapshots[6] or by direct approximation of the integral using the trapezoidal or Simpson's rule.[33] Both methods reformulate (21) as a matrix eigenvalue problem which can then be solved numerically by standard methods, giving virtually identical results for the plane Couette flow dataset. This was implemented in FORTRAN90 using the LAPACK[34] numerical linear algebra package.

C. POD modes for plane Couette flow

POD modes were obtained using 1000 snapshots (before averaging over the D_2 symmetry) from a single well-resolved DNS of turbulent plane Couette flow at $Re = 400$. (This is just beyond the critical Reynolds number $Re_c = 370 \pm 10$ at which sustained turbulence arises through a more natural transition, as opposed to transitions in response to special perturbations.[35]) The code uses Fourier modes in the streamwise and spanwise directions, and Legendre collocation in the wall normal direction to produce the $\mathbf{F}(n_x, n_y; z, t)$'s of (15). Pressure terms were treated by a Lagrange method.[12,36]

Table I shows the eigenvalues associated with the first thirteen (sets of) POD modes in decreasing order of eigenvalue magnitude. Here

$$\% E_{n_x n_y}^{(n)} = \left(\lambda_{n_x n_y}^{(n)} \Big/ \sum_{m, m_x, m_y} \lambda_{m_x m_y}^{(m)} \right) \times 100$$

is the percentage of average total energy contained in the (n, n_x, n_y) POD mode. Note that for consistency in a model obtained by Galerkin projection of the governing equations, if modes with n_x are included, then modes with $-n_x$ must also be included (similarly for n_y). Since, for example, *each*

TABLE I. Eigenvalues for the POD modes.

(n,n_x,n_y)	$\lambda^{(n)}_{n_x n_y}$	$\lambda^{(n)}_{n_x n_y}/\lambda^{(1)}_{00}$	$\% E^{(n)}_{n_x n_y}$
$(1,0,0)$	8.9246	1.0000	57.47
$(1,0,\pm2)$	0.5804	0.0650	3.74
$(1,0,\pm1)$	0.2807	0.0315	1.81
$(1,\pm1,\pm2)$	0.0846	0.0095	0.54
$(1,0,\pm3)$	0.0639	0.0072	0.41
$(1,\pm1,\pm1)$	0.0522	0.0058	0.34
$(2,0,\pm2)$	0.0499	0.0056	0.32
$(2,0,\pm1)$	0.0489	0.0055	0.31
$(1,\pm1,\pm3)$	0.0479	0.0054	0.31
$(2,0,\pm3)$	0.0361	0.0040	0.23
$(2,\pm1,\pm2)$	0.0346	0.0039	0.22
$(1,\pm2,\pm2)$	0.0330	0.0037	0.21
$(1,0,\pm4)$	0.0325	0.0036	0.21
...			

of the $(1,0,2)$ and $(1,0,-2)$ modes account for 3.74% of the average total energy, together these modes account for 7.48%.

Following AHLS, the ODE low-dimensional models considered in this paper will only involve projections onto POD modes lacking streamwise variations (i.e., with $n_x=0$; here we briefly describe the structures of such modes, derived via careful analysis of the symmetries (5)–(8). The $(n,0,0)$ modes can be taken to be purely real, and nonzero *only* in the x or the y component, and are either odd or even under $z \to -z$. The $(1,0,0)$ mode contains over half (57.47%) of the total average energy, and, as shown in Fig. 1, approximates the experimentally and numerically observed mean turbulent velocity profile with higher velocity gradient near the walls and lower gradients toward the center;[37,38] the remaining $(n,0,0); n \geq 2$ modes contribute only 0.7% to this mean. The x and z components of $\phi^{(n)}_{0n_y}$ can without loss of generality be taken to be real, with the y component purely imaginary.[39] Also, symmetry arguments show that either the
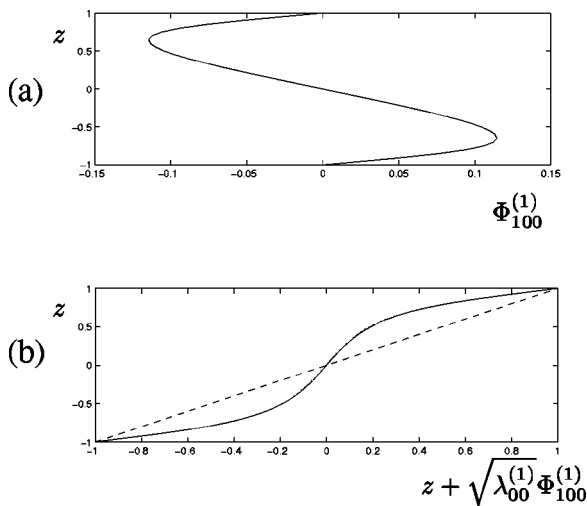

FIG. 1. (a) The x component of the POD mode $\Phi^{(1)}_{00}$. The y and z components are equal to zero. (b) The velocity profile obtained by adding this POD mode with its r.m.s. amplitude $\sqrt{\lambda^{(1)}_{00}} = \sqrt{\langle|a^{(1)}_{00}(t)|^2\rangle}$ [cf. (14)] to the laminar state $\mathbf{U}_0 = z\mathbf{e}_x$. This lies within 0.7% of the mean flow obtained from the full DNS ensemble average (dotted curve, barely visible).
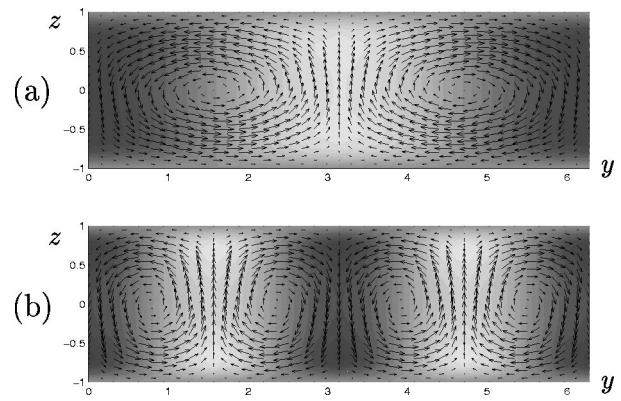

FIG. 2. Flow fields **u** associated with the (a) $(n,n_x,n_y)=(1,0,1)$ and (b) $(1,0,2)$ POD modes. The vectors show the spanwise and wall normal components of the velocity, while the dark (light) shading denotes positive (negative) streamwise velocity.

x and z components are even and the y component odd, or that the x and z components are odd and the y components even under $z \to -z$. The $(1,0,n_y)$ POD modes consist of n_y (spanwise) pairs of streamwise rolls and associated streaks, henceforth called "roll modes" (see Fig. 2); $(n,0,n_y)$ modes with $n>1$ and $n_y \neq 0$ have multiple layers of streamwise vortices and streaks (see Fig. 3).

The eigenvalues succeeding the five leading entries of Table I remain almost flat as n,n_x,n_y increase, so criteria for inclusion of modes in low-dimensional model cannot be purely energetic. In Sec. IV we use the modal interaction structure determined by the symmetries of the $\phi^{(n)}_{0n_y}$ in choosing specific truncations.

It is not surprising that streamwise vortices and their associated streaks are important coherent structures for turbulent PCF. As mentioned in the Introduction, such structures have been found numerically as unstable steady solutions of the NSE[10–12] (these finite amplitude solutions have some variation in the streamwise direction, but nonetheless have a strong resemblance to $n_x=0$ POD modes, which can be seen as streamwise-averaged versions of them). They can be stabilized by spatially forcing the flow with a stationary wire or bead.[40–43] They are also involved in the self-
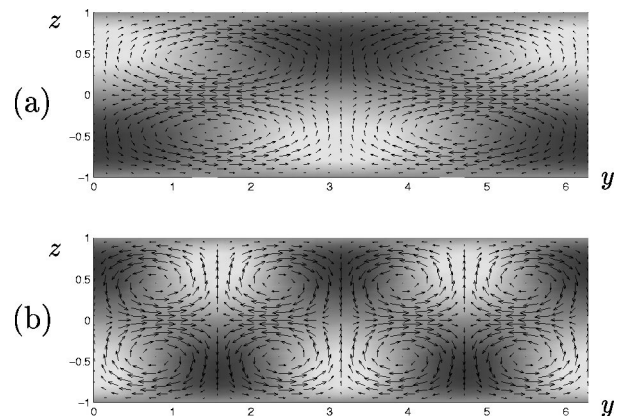

FIG. 3. Flow fields **u** associated with the (a) $(n,n_x,n_y)=(2,0,1)$ and (b) $(2,0,2)$ POD modes.

sustaining process elucidated in Refs. 14, 15, 17, and 18, although there, separate modes are associated with rolls and streaks. Here the relative roll and streak magnitudes are fixed by each vector eigenfunction $\phi_{n_x n_y}^{(n)}(z)$, but the ODEs of Sec. IV permit scale selection and roll and streak adjustment via dynamical interactions among the modal amplitudes $a_{n_x n_y}^{(n)}(t)$. In the following section, we derive models which determine dynamical interactions of such streamwise vortices.

IV. LOW-DIMENSIONAL MODELS

Inserting (10) into (1) and performing a Galerkin projection[7] we obtain an infinite set of ODEs of the form

$$\dot{a}_{k_x k_y}^{(k)} = \sum_{n=1}^{\infty} \hat{A}_{k_x k_y}^{(k,n)} a_{k_x k_y}^{(n)} + [N(\mathbf{a},\mathbf{a})]_{k k_x k_y}, \tag{22}$$

where

$$[N(\mathbf{a},\mathbf{a})]_{k k_x k_y} = \sum_{\substack{m,n, \\ m_x, m_y}} \hat{B}_{k_x k_y m_x m_y}^{(k,m,n)} a_{m_x m_y}^{(m)} a_{k_x - m_x, k_y - m_y}^{(n)},$$

$$k = 1,2,\ldots, \quad k_x, k_y = \ldots, -2, -1, 0, 1, 2, \ldots .$$

Finite dimensional models are obtained by truncating (22). The $\hat{A}$'s and $\hat{B}$'s are calculated from integrals of products of components of POD modes and their derivatives; explicit expressions are given in Appendix B. Equation (13) implies that we need only explicitly include approximately half of the variables $a_{k_x k_y}^{(k)}$. Note that the $\hat{A}$'s contain Re as a parameter; our POD modes are *optimal* at $Re = 400$, but the NSE can be projected onto them for *any* Re.

Through multiplication by appropriate complex constants, the POD modes may be chosen so that the actions of the group elements given in (5)–(8) on the amplitudes take the simple forms

$$\mathcal{P}: a_{n_x n_y}^{(n)}(t) \rightarrow \pm a_{-n_x - n_y}^{(n)}(t),$$

$$\mathcal{R}: a_{n_x n_y}^{(n)}(t) \rightarrow \pm a_{n_x - n_y}^{(n)}(t),$$

$$\mathcal{RP}: a_{n_x n_y}^{(n)}(t) \rightarrow \pm a_{-n_x n_y}^{(n)}(t), \tag{23}$$

$$\mathcal{T}_{\Delta x}: a_{n_x n_y}^{(n)}(t) \rightarrow e^{in_x \phi_x} a_{n_x n_y}^{(n)}(t),$$

$$\mathcal{T}_{\Delta y}: a_{n_x n_y}^{(n)}(t) \rightarrow e^{in_y \phi_y} a_{n_x n_y}^{(n)}(t).$$

Here the choice of $\pm$ depends on n_x, n_y, and n in an empirically determined fashion, and $\phi_x \equiv 2\pi \Delta x/L_x$, $\phi_y \equiv 2\pi \Delta y/L_y$. The ODEs (22) will be equivariant with respect to these group actions, i.e., writing (22) as $\dot{\mathbf{a}} = f(\mathbf{a})$, it is necessary that $f(\gamma \mathbf{a}) = \gamma f(\mathbf{a})$ for all $\gamma \in O(2) \times O(2)$.[44,45] This can be interpreted as limiting the nonzero terms which appear in (22). Also, by exploiting symmetry properties of the POD modes (specifically, oddness or evenness of components $\phi_{in_x n_y}^{(n)}$ under $z \rightarrow -z$), it can be shown that more of the $\hat{A}$'s and $\hat{B}$'s vanish identically. Finally, there are further

conditions on the $\hat{B}$'s arising from the fact that the nonlinear terms in the Navier–Stokes equations are energy-conserving. Specifically

$$\int\int\int_\Omega \mathbf{u} \cdot (\mathbf{u} \cdot \nabla \mathbf{u}) d^3\mathbf{x}$$

$$= \int\int\int_\Omega \mathbf{u}(\nabla(\tfrac{1}{2}\mathbf{u}\cdot\mathbf{u}) - \mathbf{u} \times (\nabla \times \mathbf{u})) d^3\mathbf{x}$$

$$= \int\int\int_\Omega \nabla \cdot ((\tfrac{1}{2}\mathbf{u}\cdot\mathbf{u})\mathbf{u}) d^3\mathbf{x}$$

$$= \int\int_{\partial\Omega} (\tfrac{1}{2}\mathbf{u}\cdot\mathbf{u})\mathbf{u}\cdot\hat{\mathbf{n}}dS = 0, \tag{24}$$

where we have used vector identities, the facts that $\mathbf{u} \cdot (\mathbf{u} \times (\nabla \times \mathbf{u})) = 0$ and $\nabla \cdot \mathbf{u} = 0$, and the divergence theorem. The surface integral vanishes from the no-slip boundary conditions at $z = \pm 1$ and periodicity in the x and y directions. Using (10), it can be shown that Eq. (24) is equivalent to

$$\sum_{k=1}^{\infty} \sum_{k_x=-\infty}^{\infty} \sum_{k_y=-\infty}^{\infty} a_{k_x k_y}^{(k)*} [N(\mathbf{a},\mathbf{a})]_{k k_x k_y} = 0. \tag{25}$$

Equation (25) and the symmetries (23) provide checks on the nonlinear coefficients: in all cases we have found that (25) is satisfied to 0.01%.

The ODEs (22) are similar to those of the turbulent boundary layer problem in AHLS. However, there are several important differences. In AHLS, in place of $\mathbf{U}_0 = z\mathbf{e}_x$, the analog of (1) involves a spatially averaged (t-dependent) mean turbulent velocity; this was modeled as a balance between the effects of pressure and those of the coherent structures, giving cubic terms in the ODEs. No such modeling is required here: The nonlinear terms derive directly from the NSE and the $n_x = n_y = 0$ modes represent turbulent modifications to the mean, cf. Fig. 1. Second, the contribution from the pressure term at the outer edge of the wall layer was modeled as stochastic forcing in AHLS; here, it makes no contribution because of the divergence-free expansion (10) and no-slip and periodic conditions at the boundaries of Ω.[7] Third, in AHLS an eddy viscosity parameter was included to account for energy transfer to neglected modes (in fact, this was treated as a bifurcation parameter); such modeling is not included at this stage, and Re is treated as the bifurcation parameter. Finally, in AHLS the ODEs are equivariant under $O(2) \times S^1$; here, the additional reflection and rotation symmetries noted in Sec. II make the ODEs equivariant under $O(2) \times O(2)$, with actions as given above in (23), further constraining the modal interactions.

A. High-dimensional models, tracking, and energy budgets

To confirm the validity of the POD and Galerkin procedure to derive models for turbulent PCF, we first consider truncations which retain a large number of terms, specifically: All modes with $|k_x| + |k_y| \le 6$ and $1 \le k \le K$, with $K = 8$ (resp. $K = 15$), corresponding to eight real and 336 independent complex modes (resp. 15 and 630). In both cases, these modes include over 99% of the average total energy.
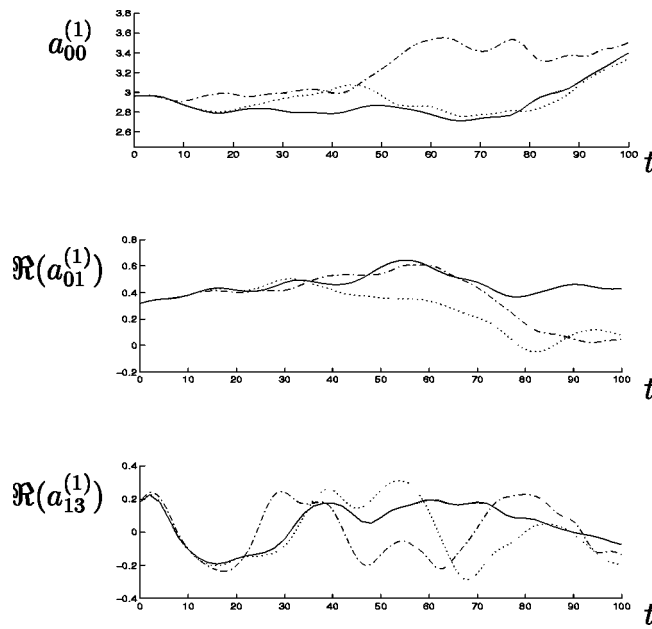
FIG. 4. Tracking performance for the $a_{00}^{(1)}$, $a_{01}^{(1)}$, and $a_{13}^{(1)}$ modes. Solid, dash–dotted and dotted lines respectively show the DNS, $K=8$ and $K=15$ model results.

We project the DNS data to get modal time histories $a_{k_x,k_y}^{(k)}(t)$, and then integrate the models from the same initial conditions. Typical results are shown in Fig. 4, from which we see that good short-term tracking is achieved for ≈ 10 (resp. 25) nondimensional time units; the time scales of these modes also appear to be correctly reproduced. We note that sensitive dependence on initial conditions precludes long-term tracking, irrespective of the order of truncation. Similar results were obtained for all other modal coefficients.

The models were then integrated for 2000 time units, the same duration as the DNS, and the values of $\langle |a_{n_x,n_y}^{(n)}|^2 \rangle$ compared. The results for the most energetic modes are given in Table II. We observe reasonable agreement, improving as K increases, with the possible exception of the $a_{0,2}^{(1)}$ mode.

In the following, we consider much more drastic truncations than these. While they necessarily neglect important effects, including energy transport through higher modes, the dynamics of such low-dimensional models can be understood in considerable detail, and, as we shall see, they suggest that sustained PCF turbulence is associated with chaos and heteroclinic cycles in phase space.

TABLE II. Comparison of $\langle |a_{n_x,n_y}^{(n)}|^2 \rangle$ values.

(n,n_x,n_y)	$K=8$ model	$K=15$ model	DNS data
(1,0,0)	11.0205	8.8361	8.9246
(1,0,±2)	0.0928	0.3105	0.5804
(1,0,±1)	0.1582	0.2842	0.2807
(1,±1,±2)	0.0662	0.0793	0.0846
(1,0,±3)	0.0457	0.0795	0.0639
(1,±1,±1)	0.0667	0.0537	0.0522
(2,0,±2)	0.0377	0.0449	0.0499
(2,0,±1)	0.0281	0.0359	0.0489
(1,±1,±3)	0.0495	0.0569	0.0479
...			

TABLE III. Coefficients for Eqs. (26) and (27) for $N_y=6$.

j	A_j'	A_j''	B_j
0	⋯	11.4349	⋯
1	0.0688	5.5563	0.0117
2	0.1738	10.8038	0.0264
3	0.2218	15.3067	0.0325
4	0.2414	22.0804	0.0336
5	0.2324	30.2181	0.0339
6	0.1968	41.0443	0.0289

B. Models with $k=1$ and $k_x=0$

In AHLS, a ten-dimensional system of ODEs modeling the turbulent boundary layer was derived and studied; that model would correspond in the present notation to the truncation of the analog of (22) with $k=1$, $k_x=0$, $-5 \leq k_y \leq 5$. Inspired by the success of that model in capturing certain features of boundary layer turbulence, we first consider (22) for the truncation $k=1$, $k_x=0$, $-N_y \leq k_y \leq N_y$. For $N_y=2$ this is the leading triad of Table I.

Letting $r_0 = a_{00}^{(1)} \in R$ and $a_{0j}^{(1)} \equiv r_j e^{i\theta_j}$, $r_j \geq 0$ for $j=1,...,N_y$, we obtain

$$\dot{r}_0 = A_0 r_0 + 2 \sum_{q=1}^{N_y} B_q r_q^2, \tag{26}$$

$$\dot{r}_j = (A_j - B_j r_0) r_j, \quad j=1,...,N_y, \tag{27}$$

$$\dot{\theta}_j = 0, \quad j=1,...,N_y. \tag{28}$$

Here A_0, the A_j's, and the B_q's are real, and the former have the forms

$$A_0 \equiv -A_0''/Re, \quad A_j \equiv A_j' - A_j''/Re; \quad j \geq 1, \tag{29}$$

where the A_j''s, A_j'''s and B_q's are positive (see Table III); in particular A_0 is always negative. For asymptotic behavior, at fixed Re we need only consider modes with $A_j>0$; $j \geq 1$, because (26) and positivity of the B_q's imply that $r_0<0$ gives $\dot{r}_0>0$. Thus, eventually the system evolves to a state with $r_0>0$, and then, from (27), modes with $A_j<0$ asymptotically decay to zero.

Equations (26) and (27) have the trivial fixed point P_0 defined by $r_j=0$ for all j, corresponding physically to the laminar state. Its eigenvalues $A_0, A_1,...,A_{N_y}$ show that it is linearly unstable if any A_j is positive for $j \geq 1$. Equations (26) and (27) also have nontrivial fixed points P_l for $l=1,...,N_y$ defined by $r_l=(-A_0 A_l/(2B_l^2))^{1/2}$, $r_0=A_l/B_l$, and $r_j=0$ for $j \neq 0,l$. [From (28), each P_l represents a circle of fixed points in terms of the original amplitudes $a_{0j}^{(1)}$, corresponding to spanwise translations $\mathcal{T}_{\Delta y}$ of the velocity field.] The eigenvalues of these fixed points are

$$\mu_{\pm}^{(l)} \equiv (A_0 \pm (A_0^2 + 8A_0 A_l)^{1/2})/2, \tag{30}$$

corresponding to perturbations in the (r_0, r_l) plane, and

$$\mu_q^{(l)} \equiv A_q - B_q A_l/B_l, \quad q \neq 0,l,$$

corresponding to perturbations in the r_q-direction. The P_l fixed points represent states in which the mean flow is coupled to streamwise vortices and their associated streaks.

TABLE IV. Fixed point properties for $N_y = 6$.

Fixed Pt	Existence	Stable range
P_0	all Re	$Re < 62.16$
P_1	$Re > 80.76$	$\cdots$
P_2	$Re > 62.16$	$62.16 < Re < 255.89$
P_3	$Re > 69.01$	$255.89 < Re < 517.30$
P_4	$Re > 91.47$	$Re > 517.30$
P_5	$Re > 130.03$	$\cdots$
P_6	$Re > 208.56$	$\cdots$

Such states strongly resemble those associated with stable fixed points for the model considered in Refs. 15 and 16. Note that $r_0 > 0$ implies a "turbulent" mean flow profile similar to that discussed in Refs. 37 and 38; cf. Fig. 1 above.

We have the following general result:

The system (26) and (27) with $A_0 > 0$ and $A_j > 0, B_j > 0$ for $j = 1, \ldots, N_y$ has at least one, and generically only one, linearly stable nontrivial fixed point.

Stability is shown by induction. Suppose $N_y = 1$. The fixed point P_1 has eigenvalues $\mu_{\pm}^{(1)}$ which both have negative real part. Now suppose for the truncation at N_y that there is a linearly stable nontrivial fixed point, say P_L. The eigenvalues of P_L are $\mu_{\pm}^{(L)}$, both with negative real part, and

$$\mu_q^{(L)} < 0, \quad q = 1, 2, \ldots, L-1, L+1, \ldots, N_y. \tag{31}$$

For the truncation at $N_y + 1$, P_L has an additional eigenvalue $\mu_{N_y+1}^{(L)}$. If this is negative then P_L is linearly stable and the result follows, so suppose instead that $\mu_{N_y+1}^{(L)} > 0$. The fixed point P_{N_y+1} has eigenvalues $\mu_{\pm}^{(N_y+1)}$, both with negative real part, and $\mu_q^{(N_y+1)}$, $q = 1, \ldots, N_y$. By explicit computation

$$\mu_L^{(N_y+1)} = -\frac{B_L}{B_{N_y+1}} \mu_{N_y+1}^{(L)} < 0.$$

Finally, $\mu_{N_y+1}^{(L)} > 0$ implies that $A_{N_y+1}/B_{N_y+1} > A_L/B_L$, so

$$A_q - B_q A_{N_y+1}/B_{N_y+1} < A_q - B_q A_L/B_L = \mu_q^{(L)},$$

and using (31), we conclude that

$$\mu_q^{(N_y+1)} < 0, \quad q = 1, 2, \ldots, L-1, L+1, \ldots, N_y.$$

Thus, P_{N_y+1} is linearly stable.

As an example, consider Eqs. (26) and (27) with $N_y = 6$, which captures 70.17% of the average total energy (albeit omitting more energetic modes than some of those included). The coefficients and fixed point properties are given in Tables III and IV, respectively. (Here and henceforth, we specify coefficients to four decimal places: at this order the "conservative" constraint (25) is always satisfied. All of the results which we report are robust to small changes in these coefficients.) The exchange of stability between the P_3 and P_4 fixed points at $Re = 517.30$ may be understood by considering a restriction to $r_1 = r_2 = r_5 = r_6 = 0$ [from (27) this is an invariant subspace, meaning that if the system starts in this subspace, it remains there for all time]. The reduced equations are

$$\dot{r}_0 = A_0 r_0 + 2B_3 r_3^2 + 2B_4 r_4^2, \tag{32}$$

$$\dot{r}_3 = (A_3 - B_3 r_0) r_3, \tag{33}$$

$$\dot{r}_4 = (A_4 - B_4 r_0) r_4. \tag{34}$$

At the exchange of stability, $\mu_3^{(4)} = \mu_4^{(3)} = 0$, so $A_3/B_3 = A_4/B_4$. At $r_0 = A_3/B_3 = A_4/B_4$, we thus have $\dot{r}_3 = \dot{r}_4 = 0$, and at this value of r_0, $\dot{r}_0 = 0$ for

$$2B_3 r_3^2 + 2B_4 r_4^2 = A_0 A_3/B_3. \tag{35}$$

Thus, there are fixed points at $(r_0, r_1, r_2, r_3, r_4, r_5, r_6) = (A_3/B_3, 0, 0, r_3, r_4, 0, 0)$ for all r_3 and r_4 satisfying (35): this is an (elliptical) arc of fixed points connecting P_3 to P_4. Similar behavior occurs at the exchange of stability at $Re = 255.89$. Only at such bifurcation values of Re do multiple stable equilibria exist.

Note that, in view of (28), each $r_j \neq 0$ fixed point actually belongs to a *circle* of equilibria. Reference to Figs. 2 and 3 shows that this corresponds to families of streamwise vortices and streaks at arbitrary spanwise locations.

These "minimal" models suggest a simple interpretation of the mechanism that sustains nontrivial behavior in PCF (we hesitate to call it turbulence in this context). Recall that r_0 is the amplitude of the (modification to) the mean flow $\Phi_{00}^{(1)}(\mathbf{x})$, which, for $r_0 > 0$, promotes the inflection-point profiles observed in turbulent PCF (Fig. 1), and that r_j; $j \geqslant 1$ are the amplitudes of the modes containing streamwise vortices (Fig. 2). From Equation (26) we see that the collective magnitudes of the latter drive the former, which would otherwise decay. In turn, (some of) the roll modes r_j are linearly unstable for small r_0, but excessive growth in r_0 leads to decay in the r_j [Eq. (27)], setting up a self-sustaining and self-limiting process, much as in the model of Waleffe.[14–16,18] However, as shown above, for almost all coefficients $A_j, B_j > 0$, the flow of Eqs. (26) and (27) tends to a stable fixed point at $(r_0, r_l, r_q) = (A_l/B_l, (-A_0 A_l/(2B_l^2))^{1/2}, 0)$, where $A_l/B_l > A_q/B_q$ for all $q \neq 0, l$ [cf. (30)]. This is the unique attractor for the two-dimensional invariant subspace spanned by r_0 and r_l, and on which the dynamics are simply given by

$$\dot{r}_0 = A_0 r_0 + 2B_l r_l^2, \quad \dot{r}_l = (A_l - B_l r_0) r_l. \tag{36}$$

Thus only the "least stable" roll mode remains active. As we shall see, addition of two members of the second (quantum) family of modes significantly enriches this picture.

It must be noted that these models incorrectly predict that the laminar state P_0 becomes linearly unstable for sufficiently high Re (as soon as the "first" A_j becomes positive). This comes from a well-known limitation of POD-based models: as discussed in Refs. 15 and 46 and noted in Sec. III B, models derived from sustained turbulent data using the expansion (10) necessarily couple streamwise and cross-stream disturbances, leading to instability of the laminar state. Specifically, the Re-independent components A_j' of the linear coefficients of (27), derived from the second term of (B1), are strictly positive. Indeed, for (very) low-dimensional truncations, including ones lacking streamwise modes, instability of the trivial solution is an unavoidable consequence of averaging over "active" velocity fields of the ensemble that remain relatively far from the laminar state,

Phys. Fluids, Vol. 14, No. 7, July 2002

Models for turbulent plane Couette flow   2501

and give rise to eigenfunctions with $-\int \phi_{3k_x k_y}^{(n)} \phi_{1k_x k_y}^{(k)*} dz > 0$, cf. Ref. 7. Ensembles collected for smaller Re, having longer episodes of laminar flow, would presumably give modes with $-\int \phi_{3k_x k_y}^{(n)} \phi_{1k_x k_y}^{(k)*} dz < 0$, leading to stability of the laminar state. Moreover, it is argued in Ref. 46 that models using an "unconstrained" empirical expansion derived from the POD, that decouples streamwise and cross-stream disturbances, correctly give laminar stability, and furthermore, behaviors of models derived using the expansion (10) are strongly echoed in those derived using the decoupled expansion. In short, the present model can represent sustained "turbulence," but *not* the transition from laminar flow as Re increases. Further comments on this appear in Sec. V.

C. A model including $k=2$ modes

The models of Sec. IV A can capture the sustained turbulent state quite well; however, they are of such high dimension that detailed analysis is impossible. On the other hand, the severely truncated models of Sec. IV B can be essentially completely understood, but their stable fixed points are too simple to characterize the turbulent state. Here we consider an extension of the models of Sec. IV B that lies between these extremes: Its dimension is low enough that detailed analyses can be undertaken, yet it preserves more realistic signatures of sustained turbulence. Specifically, we include the most energetic streamwise invariant modes with $k>1$, namely the $(2,0,\pm 1)$ and $(2,0,\pm 2)$ modes. Inclusion of these members of the second "quantum" family introduces new Fourier wave number interactions, the most important being those with the modes $(1,0,k_y)$ with $|k_y| \leq 4$. Truncating to include only these modes, we obtain

$$\dot{a}_0^{(1)} = A_0 a_0^{(1)} + 2 \left(\sum_{q=1}^4 B_q |a_q^{(1)}|^2 + B_1^{(2)} |a_1^{(2)}|^2 + B_2^{(2)} |a_2^{(2)}|^2 \right),$$
(37)

$$\dot{a}_1^{(1)} = (A_1 - B_1 a_0^{(1)}) a_1^{(1)} - C_{1,12} a_1^{(1)*} a_2^{(2)} + C_{1,32} a_3^{(1)} a_2^{(2)*} - C_{1,21} a_2^{(1)} a_1^{(2)*},$$
(38)

$$\dot{a}_2^{(1)} = (A_2 - B_2 a_0^{(1)}) a_2^{(1)} + C_{2,42} a_4^{(1)} a_2^{(2)*} - C_{2,11} a_1^{(1)} a_1^{(2)} - C_{2,31} a_3^{(1)} a_1^{(2)*},$$
(39)

$$\dot{a}_3^{(1)} = (A_3 - B_3 a_0^{(1)}) a_3^{(1)} + C_{3,12} a_1^{(1)} a_2^{(2)} - C_{3,21} a_2^{(1)} a_1^{(2)} - C_{3,41} a_4^{(1)} a_1^{(2)*},$$
(40)

$$\dot{a}_4^{(1)} = (A_4 - B_4 a_0^{(1)}) a_4^{(1)} + C_{4,22} a_2^{(1)} a_2^{(2)} - C_{4,31} a_3^{(1)} a_1^{(2)},$$
(41)

$$\dot{a}_1^{(2)} = (A_1^{(2)} - B_1^{(2)} a_0^{(1)}) a_1^{(2)} + (C_{1,21} + C_{2,11}) a_2^{(1)} a_1^{(1)*} + (C_{2,31} + C_{3,21}) a_3^{(1)} a_2^{(1)*} + (C_{3,41} + C_{4,31}) a_4^{(1)} a_3^{(1)*} - C_{2,11}^{(2)} a_2^{(2)} a_1^{(2)*},$$
(42)

$$\dot{a}_2^{(2)} = (A_2^{(2)} - B_2^{(2)} a_0^{(1)}) a_2^{(2)} + C_{1,12} (a_1^{(1)})^2 - (C_{3,12} + C_{1,32}) a_1^{(1)*} a_3^{(1)} - (C_{2,42} + C_{4,22}) a_2^{(1)*} a_4^{(1)} + C_{2,11}^{(2)} (a_1^{(2)})^2.$$
(43)

Here we have suppressed the subscript $k_x=0$ of the a's and simplified the notation of (22), as in (26)–(28). The coefficients A_0 and $A_j, B_j; 1 \leq j \leq 4$ are given by (29) and Table III; the additional coefficients are

$$A_1^{(2)} = 0.0323 - 12.0680/Re,$$

$$A_2^{(2)} = 0.1062 - 15.9763/Re,$$

$$B_1^{(2)} = 0.0028, \quad B_2^{(2)} = 0.0077,$$

$$C_{1,12} = 0.0098, \quad C_{1,21} = 0.0164,$$

$$C_{1,32} = 0.0165, \quad C_{2,11} = 0.0209,$$

$$C_{2,31} = 0.0167, \quad C_{2,42} = 0.0105,$$

$$C_{3,12} = 0.0302, \quad C_{3,21} = 0.0439,$$

$$C_{3,41} = 0.0204, \quad C_{4,22} = 0.0613,$$

$$C_{4,31} = 0.0471, \quad C_{2,11}^{(2)} = 0.0064.$$

This model includes the leading modes lacking streamwise variations, cf. Table I, and its structure remains similar when more modes with $k_x=0$ are included.

Some preliminary notes are in order. First, the $\{a_1^{(2)} = 0\}$ and $\{a_2^{(2)} = 0\}$ subspaces are *not* invariant: $a_1^{(2)}$ and $a_2^{(2)}$ can be excited by nonlinear interactions among the $a_{k_y}^{(1)}$ modes. Other $k \neq 1$ modes not included in this truncation can be similarly excited, but these contain a smaller fraction of the average kinetic energy, and hence are presumably less important, and their exclusion simplifies the analysis. Second, the dynamics of this model typically fail to satisfy the energy budgets of Table I, presumably because significant energy-transferring interactions are absent. In AHLS (see also Ref. 24) this problem was partially overcome through the introduction of a Heisenberg-type model to account for energy losses to neglected modes. This requires determination of additional parameters; for simplicity, we do not model neglected modes here, so that our only parameter is the Reynolds number Re. As we will see, Eqs. (37)–(43) exhibit interesting behavior for $350 \lesssim Re \lesssim 600$.

To understand these dynamics, we first observe that Eqs. (37)–(43) have a hierarchy of invariant subspaces as given in Table V. For example, $\mathcal{S}_e^R \subset \mathcal{S}_e$ is the "real" subspace obtained by restricting the amplitudes in the "even" subspace $\mathcal{S}_e$ to being real (recall that $a_0^{(1)}$ is always real). Real subspaces correspond to velocity fields symmetric under the spanwise and pointwise reflections $\mathcal{R}$ and $\mathcal{P}$, as follows from (13) and (23) with $n_x=0$. Acting on the invariant subspaces $\mathcal{S}_e^R$, $\mathcal{S}_o^R$, $\mathcal{S}_{012}^R$, $\mathcal{S}_2$, $\mathcal{S}_3$, $\mathcal{S}_4$, and $\mathcal{S}_2^{(2)}$ with $S^1(\mathcal{T}_{\Delta y})$ gives invariant subspaces which are rotated (i.e., spanwise translated) copies of the originals.

The fixed points P_2, P_3, and P_4 of Sec. IV B can be shown to persist for (37)–(43) by restricting to the subspaces $\mathcal{S}_2$, $\mathcal{S}_3$, and $\mathcal{S}_4$, respectively. An analogous nontrivial fixed

TABLE V. Invariant subspaces for Eqs. (37)–(43): Variables not identified in $\{\cdots\}$ remain zero.

Invariant subspace	Dimension
$\mathcal{S}_e \equiv \{a_0^{(1)}, a_2^{(1)}, a_4^{(1)}, a_2^{(2)}\}$	7
$\mathcal{S}_o \equiv \{a_0^{(1)}, a_1^{(1)}, a_3^{(1)}, a_2^{(2)}\}$	7
$\mathcal{S}_{012} \equiv \{a_0^{(1)}, a_1^{(2)}, a_2^{(2)}\}$	5
$\mathcal{S}_e^R \equiv \{a_0^{(1)}, \Re(a_2^{(1)}), \Re(a_4^{(1)}), \Re(a_2^{(2)})\}$	4
$\mathcal{S}_o^R \equiv \{a_0^{(1)}, \Re(a_1^{(1)}), \Re(a_3^{(1)}), \Re(a_2^{(2)})\}$	4
$\mathcal{S}_{012}^R \equiv \{a_0^{(1)}, \Re(a_1^{(2)}), \Re(a_2^{(2)})\}$	3
$\mathcal{S}_2 \equiv \{a_0^{(1)}, \Re(a_2^{(1)})\}$	2
$\mathcal{S}_3 \equiv \{a_0^{(1)}, \Re(a_3^{(1)})\}$	2
$\mathcal{S}_4 \equiv \{a_0^{(1)}, \Re(a_4^{(1)})\}$	2
$\mathcal{S}_2^{(2)} \equiv \{a_0^{(1)}, \Re(a_2^{(2)})\}$	2

point $P_2^{(2)} \in \mathcal{S}_2^{(2)}$ also exists for sufficiently high Re (≥ 150.44). Note that $\{a_0^{(1)}, \Re(a_1^{(1)})\}$ and $\{a_0^{(1)}, \Re(a_1^{(2)})\}$ are *not* invariant subspaces; "pure" P_1 and $P_1^{(2)}$ fixed points do not exist for (37)–(43). As above, all fixed points lie on circles of equilibria obtained under the action of $S^1(\mathcal{T}_{\Delta y})$.

We first consider the $\mathcal{S}_{012}$ subspace, on which Eqs. (37)–(43) reduce to

$$\dot{a}_0^{(1)} = A_0 a_0^{(1)} + 2(B_1^{(2)}|a_1^{(2)}|^2 + B_2^{(2)}|a_2^{(2)}|^2), \qquad (44)$$

$$\dot{a}_1^{(2)} = (A_1^{(2)} - B_1^{(2)} a_0^{(1)}) a_1^{(2)} - C_{2,11}^{(2)} a_2^{(2)} a_1^{(2)*}, \qquad (45)$$

$$\dot{a}_2^{(2)} = (A_2^{(2)} - B_2^{(2)} a_0^{(1)}) a_2^{(2)} + C_{2,11}^{(2)} (a_1^{(2)})^2. \qquad (46)$$

This subspace captures the interaction of the mean flow with the $k = 2$ modes in 1:2 spatial resonance. In the region $0 < z < 1$ (or $-1 < z < 0$), this mode interaction corresponds physically to a "boundary-layer" mean flow profile interacting with streamwise rolls in 1:2 spatial resonance (cf. Figs. 1 and 3). Such an interaction has been investigated from a similar perspective for a single turbulent boundary layer in Ref. 47, although this involved modeling of the mean flow, whereas here we allow the mean flow to evolve dynamically.

We summarize the main results from a numerical bifurcation analysis (using AUTO[48]) of Eqs. (44)–(46) for the coefficients of interest. Here and elsewhere, *orbital* stability is indicated, that is, asymptotic stability with respect to perturbations within the sub-space *not* associated with the continuous symmetry $S^1(\mathcal{T}_{\Delta y})$ (which gives an eigenvalue or Floquet exponent equal to zero).[44] Our description is for increasing Re. The laminar state ($a_0^{(1)} = a_1^{(2)} = a_2^{(2)} = 0$) is stable for $Re < 150.44$; at this value, it loses stability to a circle of stable "pure mode" fixed points (with $a_0^{(1)} \neq 0$, $a_2^{(2)} \neq 0$, $a_1^{(2)} = 0$). These then lose stability at $Re = 311.86$ to a circle of stable "mixed mode" (MM) fixed points (with $a_0^{(1)} \neq 0$, $a_1^{(2)} \neq 0$, $a_2^{(2)} \neq 0$). At $Re = 339.82$, the MM fixed points lose stability to periodic traveling waves; these in turn lose stability at $Re = 340.84$ to quasiperiodic modulated traveling waves, which remain stable until $Re = 354.82$. Most interestingly, attracting, structurally stable heteroclinic cycles connecting two $\mathcal{T}_{L_y/4}$-symmetry related $P_2^{(2)}$ fixed points exist for $Re \gtrsim 346$. Near such a cycle, trajectories alternately visit the vicinities of these two unstable saddle points, with excursions in which $|a_1^{(2)}|$ grows and $|a_0^{(1)}|$ collapses between visits. Since the cycles *attract*, nearby solutions approach them,
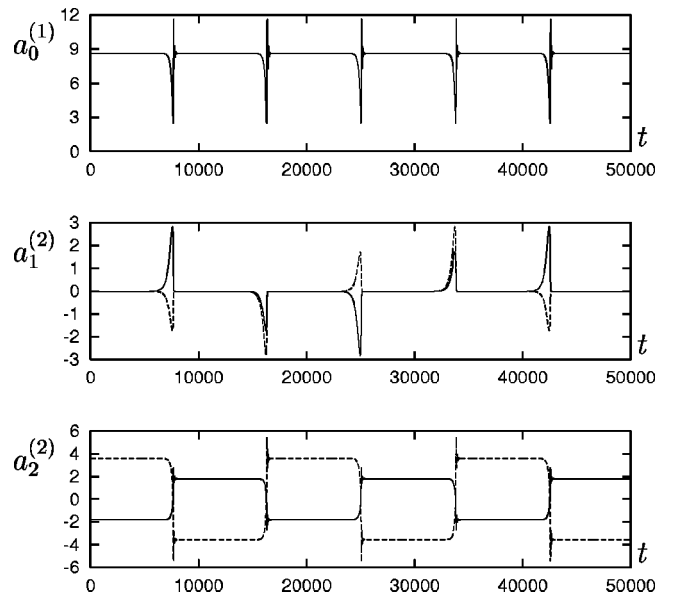

FIG. 5. Time series showing an attracting heteroclinic cycle connecting $P_2^{(2)}$ fixed points for Eqs. (37)–(43) restricted to $\mathcal{S}_{012}$ at $Re = 400$. The solid (dashed) lines show the real (imaginary) parts of the amplitudes.

and *structural stability* implies that they persist over a range of Re values, and also under small perturbations to other coefficients, as might result from different POD bases. Structural stability of these heteroclinic cycles is a consequence of the $O(2)$ symmetry for the $\mathcal{S}_{012}$ subspace inherited from periodic boundary conditions in the spanwise direction; this also implies that there is a full circle of such cycles.

The time series for such a cycle at $Re = 400$ is shown in Fig. 5, with reconstructed velocity fields at eight time instants during passage near the cycle shown in Fig. 6. As for the boundary layer model in AHLS, the pair of fixed points in each individual cycle correspond to rolls translated
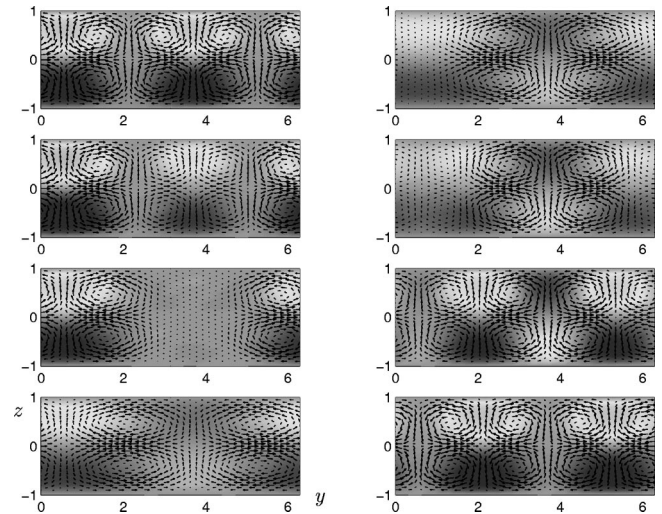

FIG. 6. Snapshots of velocity fields corresponding to part of the heteroclinic cycle of Fig. 5; same convention as Fig. 2, time increasing down left then right column. The first and last panels are near the unstable fixed points; between these the rolls and streaks interact, combine and reform with a lateral shift as the orbit follows the heteroclinic connection. Due to the restricted set of modes, flows maintain symmetry about the midplane.
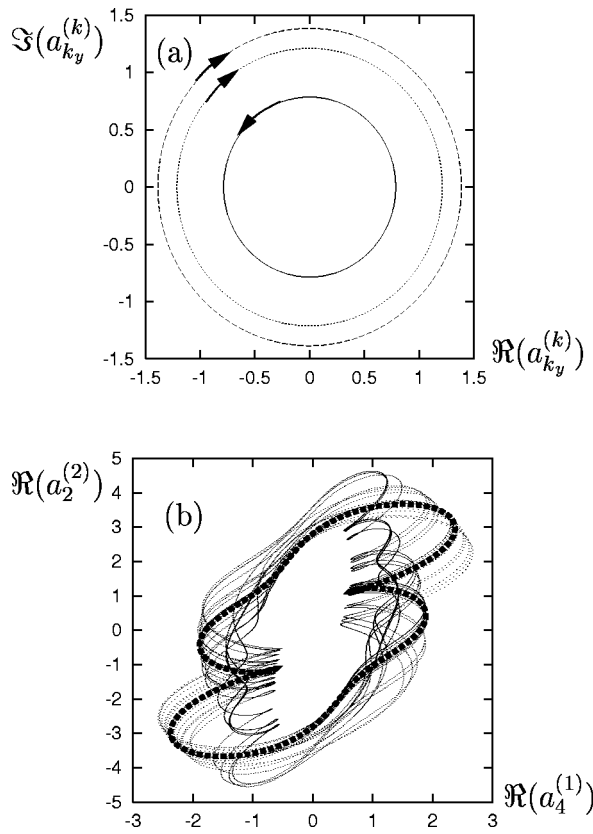
FIG. 7. Projections onto modal phase planes of solutions of Eqs. (37)–(43) restricted to the S_e subspace. (a) The stable three-torus at $Re=350$; the solid, dashed, and dotted lines correspond to $(k,k_y)=(1,2),(1,4)$, and $(2,2)$, respectively. (b) The strange attractor in S_e^R at $Re=400$. The thick dashed line shows the unstable periodic orbit which acts as the "core" of the strange attractor.
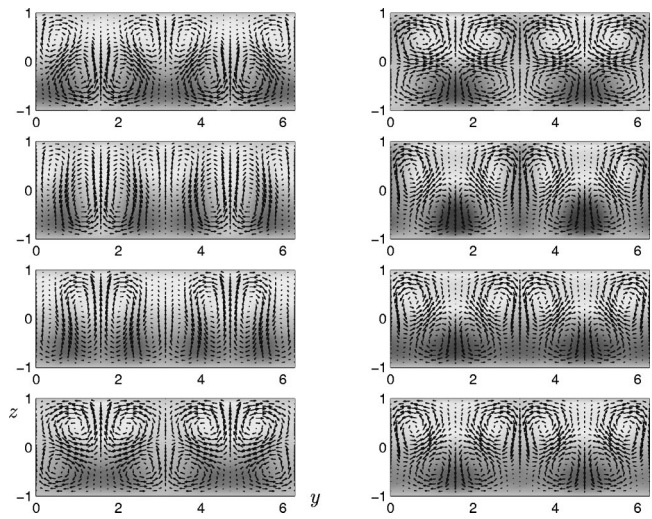

FIG. 8. Velocity fields corresponding an orbit making a half circuit on the strange attractor of Fig. 7(b). Note how the rolls grow and shrink cyclically. Since S_e contains only even spanwise wave numbers, the pattern has spanwise period π (half the box).

Similar, somewhat more complex, bifurcations occur in S_o. Here we note only that for $530 \lesssim Re \lesssim 750$, attracting, structurally stable, heteroclinic cycles connecting $\mathcal{T}_{L_y/4}$-symmetry related $P_2^{(2)}$ fixed points exist; see Fig. 9, and Fig. 10 for the reconstructed velocity fields. These cycles differ in detail from those in S_{012} described above (the excursions involve modes $|a_1^{(1)}|$ and $|a_3^{(1)}|$ in place of $|a_1^{(2)}|$), but their effects are similar in that the fixed points in each cycle are related by one-quarter-domain spanwise translation
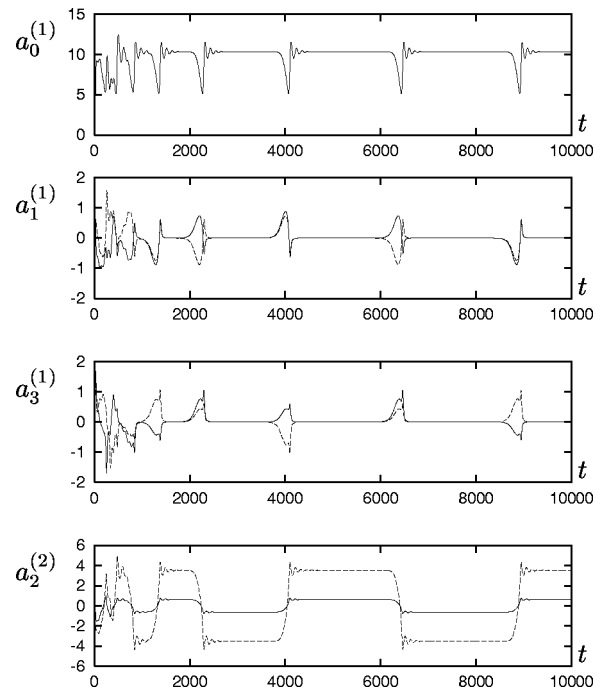
through one quarter of the spanwise domain [i.e., half a wavelength of the roll pattern, via the action of $\mathcal{T}_{L_y/4}$, cf. Fig. 3(b)]. Note that the existence and stability properties described here are analogous to those for the normal form for spatial 1:2 mode interaction *without* mean flow;[49] if $a_0^{(1)}$ is replaced by its adiabatic value obtained by setting $\dot{a}_0^{(1)}=0$, Eqs. (44)–(46) reduce exactly to that normal form.

We next describe the behavior restricted to the S_e subspace. The P_2 fixed points are stable within S_e from $Re=62.16$, where they bifurcate from the laminar state, to $Re=279.43$, where a degenerate Hopf bifurcation[50] takes place, giving rise to a branch of tori carrying quasiperiodic motions with three independent frequencies; see Fig. 7(a). The tori are stable within S_e for $255.89 \lesssim Re \lesssim 396.86$. A periodic orbit, which without loss of generality lies in S_e^R, also appears in the Hopf bifurcation. This periodic orbit branch undergoes a complicated sequence of saddle-node and period-doubling bifurcations, the latter initiating period-doubling cascades to chaos; such chaos exists for $370 \lesssim Re \lesssim 430$, and the (unstable) periodic orbit acts as the "core" of the apparent strange attractor, see Fig. 7(b), and Fig. 8 for the reconstructed velocity fields. Such attractors lie in all four-dimensional subspaces obtained under the action of $S^1(\mathcal{T}_{\Delta_y})$ on S_e^R, subspaces which are apparently attracting within S_e for all Re in this range.

FIG. 9. Time series showing an attracting heteroclinic cycle connecting $P_2^{(2)}$ fixed points for Eqs. (37)–(43) restricted to S_o at $Re=600$. The initial conditions are random, and the system quickly starts making visits near $P_2^{(2)}$ fixed points, each successive visit being longer. The solid (dashed) lines show the real (imaginary) parts of the amplitudes.
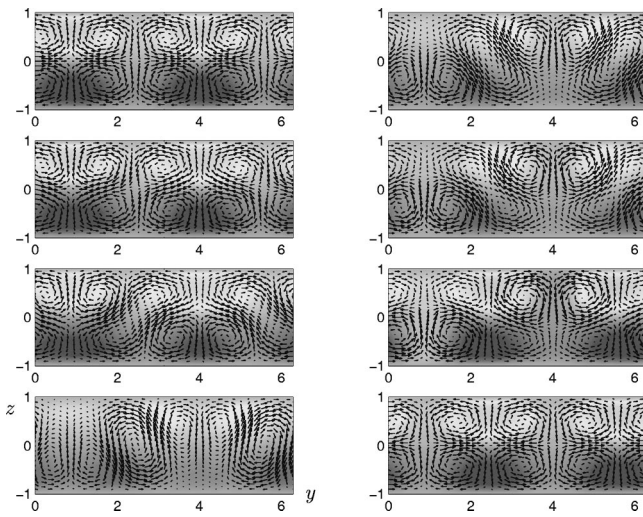
FIG. 10. Velocity fields corresponding to part of the heteroclinic cycle of Fig. 9. The first and last panels are near the unstable fixed points; between these the rolls interact and reform with a lateral shift. Note how the symmetry differs from that of Fig. 6.
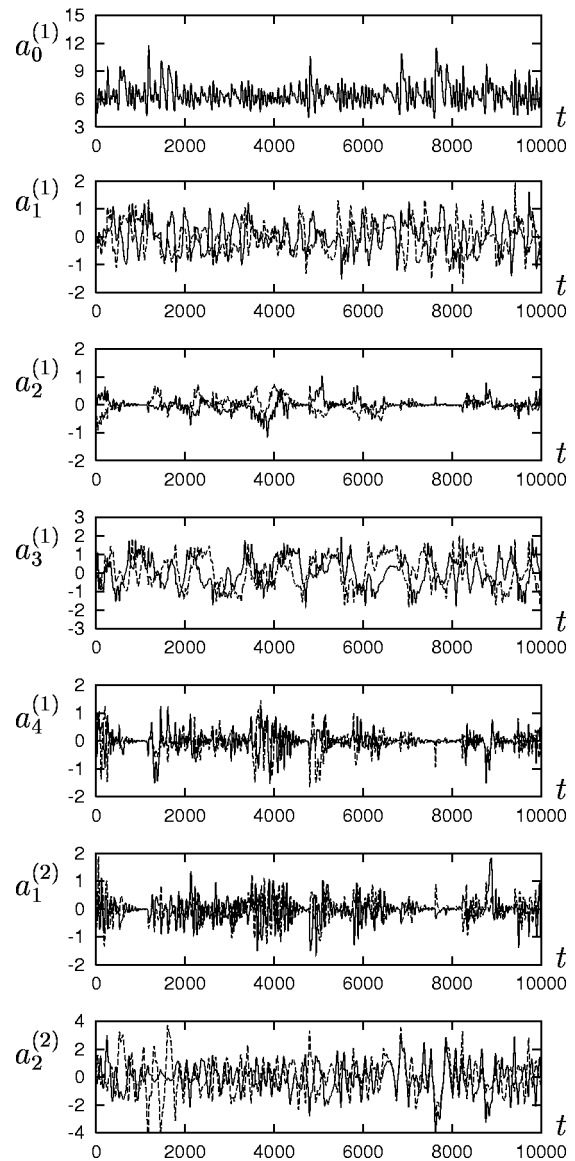

FIG. 11. Time series for solutions of Eqs. (37)–(43) in the full thirteen-dimensional state space. The solid (dashed) lines show the real (imaginary) parts of the amplitudes. Around $t = 800$ and 7500 the system makes visits near the $\mathcal{S}_o$ subspace.

of the rolls. Like the heteroclinic cycles found in the AHLS model,[4] the stable eigenvalues of $P_2^{(2)}$ in $\mathcal{S}_o$ include a complex conjugate pair corresponding to perturbations in the $\mathcal{S}_2^{(2)}$ subspace, and the cycle's attractivity is determined by eigenvalues for perturbations out of $\mathcal{S}_2^{(2)}$. Specifically, the cycle attracts when the single positive eigenvalue of $P_2^{(2)}$ has smaller magnitude than the leading (real) negative eigenvalue.

The velocity fields of Figs. 6, 8, and 10, corresponding to solutions restricted to "special" subspaces, necessarily display more symmetry than typical experimental or DNS realizations. Fields corresponding to orbits with all modes nonzero, as in Fig. 11 below, lack such clear symmetries.

A complete analysis of the full models (37)–(43) is beyond the scope of this paper. However, we do indicate the complicated relationship between the full dynamics and dynamics restricted to invariant subspaces. There are Re ranges in which each of the subspaces $\mathcal{S}_e$, $\mathcal{S}_o$, and $\mathcal{S}_{012}$ is stable for the full system, so that the remaining complex amplitudes in (37)–(43) decay to zero. For example, $\mathcal{S}_e$ is stable for $Re \approx 280$ (typical trajectories approach the three-torus in this subspace), $\mathcal{S}_o$ is stable for $Re \approx 600$, and $\mathcal{S}_{012}$ is stable for $Re \gtrsim 700$ (typical trajectories approach structurally stable heteroclinic cycles as in Figs. 9 and 5, respectively; at the lower end of the latter range small excursions out of $\mathcal{S}_{012}$ occur, but the dynamics is dominated by the $\mathcal{S}_{012}$-cycles). There are also Re ranges for which none of these subspaces are stable; for example, at $Re = 400$ typical solutions approach quasiperiodic motions involving all modes. However, even if $\mathcal{S}_o$ is unstable, chaotic solutions can exist that make intermittent visits near this subspace; see Fig. 11 for such a solution at $Re = 500$. The full dynamics of (37)–(43) are clearly complicated, but they can be partially understood in terms of behavior in lower-dimensional invariant subspaces.

The (stable) fixed points P_2, P_3, and P_4 of Sec. IV B necessarily belong to the attractors found for the full model, (cf. Table V), but the additional ($k=2$) modal interactions

present in Eqs. (37)–(43) render these simple states unstable, replacing them by dynamically active motions that "grow" from the steady states in bifurcations as Re varies. Nonetheless, observations similar to those of Sec. IV B concerning self-sustaining and self-limiting processes still hold, with the added complication that (local) stability of subspaces such as $\mathcal{S}_e$ and $\mathcal{S}_o$ is determined not only by the magnitude of $a_0^{(1)}$, but also by the nonlinear terms in (37)–(43). This permits much richer behavior, involving energy transfer among several distinct roll modes and intermittent visits to the neighborhoods of subspaces corresponding to different (spanwise) lengthscales and roll geometries.

As noted above, for such drastic truncations we cannot expect energy budgets to match those of the original data ensemble; not, at least, without models to represent losses to neglected modes. We note that the mean level of $|a_0^{(1)}|^2$ is significantly too high (33.15, compared with the DNS value

8.9246), and the mean square levels of the model's leading roll modes are correspondingly too small. Writing the kinetic energy of this model [recalling that each mode with $k_y \geqslant 1$ must be counted twice, cf. (13)]

$$E = \frac{1}{2}|a_0^{(1)}|^2 + \sum_{q=1}^{4}|a_q^{(1)}|^2 + \sum_{q=1}^{2}|a_q^{(2)}|^2, \tag{47}$$

we compute the rate of change along solutions [using (25)] as

$$\frac{dE}{dt} = A_0|a_0^{(1)}|^2 + 2\sum_{q=1}^{4}A_q|a_q^{(1)}|^2 + 2\sum_{q=1}^{2}A_q^{(2)}|a_q^{(2)}|^2. \tag{48}$$

Since (for $Re \gtrsim 150$) $A_0 < 0 < A_q, A_q^{(2)}$, net energy grows in a "cone" in state space centered on the roll modes ($|a_0^{(1)}| = 0$), and decays on a cone centered on the $a_0^{(1)}$-axis. This is clearly a poor representation of the true energy flow, which involves higher modes as well as those with streamwise variations $k_x \neq 0$. The mean flow mode $a_0^{(1)}$ is the *only* linearly dissipative mode in this model and is driven by all the other modes [cf. (37)], so it is perhaps not surprising that it equilibrates at an unrealistically high level, thus skewing the energies of the other modes. Preliminary studies indicate that the inclusion of losses to neglected modes, modeled via a Heisenberg mechanism,[4,7,24] can improve this picture.

V. CONCLUSION

In this paper, we modeled turbulent plane Couette flow by expanding the velocity field as a sum of optimal "POD modes" calculated via proper orthogonal decomposition from numerical data obtained at $Re = 400$. The most energetic mode approximates the observed mean turbulent velocity profile.[37,38] Other POD modes include pairs and stacks of streamwise rolls and associated streaks. ODE models were then obtained by Galerkin projection of the Navier–Stokes equations onto these modes. The validity of the procedure was illustrated in Sec. IV A by examining truncations that retain many terms.

We then considered two classes of low-dimensional models. For a minimal truncation including only the most energetic family of modes having no streamwise variation, the existence of linearly stable nontrivial fixed points was shown under quite general conditions (see Sec. IV B). Such fixed points correspond to states in which the mean flow is coupled to one set of streamwise vortices and their associated streaks. These roll structures resemble unstable finite amplitude solutions of the NSE,[10–12] "modes" that can be stabilized by spatially forcing the flow with a stationary wire or bead,[40–43] and structures involved in the self-sustaining process elucidated in Refs. 14–17.

When the next most energetic family of modes, still lacking streamwise variations, is included, richer dynamical behaviors are found (see Sec. IV C). Of particular interest are the attracting, structurally stable heteroclinic cycles in the $\mathcal{S}_{012}$ and $\mathcal{S}_o$ subspaces. Such cycles provide an explanation for the fact that streamwise vortices are prominent features in turbulent PCF[37] even though they are unstable: indeed, the cycles imply repeated visits near such unstable structures (cf.

Ref. 22). Moreover, these heteroclinic cycles are characterized by successive spanwise translations of rolls by half a wavelength. A similar prediction was made in AHLS[4] for the ejection and bursting events for the turbulent boundary layer; evidence for such spanwise translations was found in the experiments described in Ref. 5. For turbulent PCF, we note that Fig. 14 of Ref. 37 indicates that similar spanwise translations are associated with large velocity fluctuation events. The difference in Re and the domain's aspect ratio between those experiments and our DNS data makes direct comparison difficult; however, we hope that the present work will inspire more careful exploration of this possibility. We note that structural stability and genericity arguments[7,50] imply that these results are robust to small changes in the ODE coefficients induced by changes in empirical eigenfunctions, for example. Also, this type of geometry has been used to propose control methods to reduce the rate of "bursting" away from such sets.[51–53]

Kawahara and Kida[22] presented DNS evidence in PCF of heteroclinic cycles connecting periodic orbits that lie in a subspace analogous to $\mathcal{S}_e$, but with streamwise modes $n_x \neq 0$. They used a smaller (minimal flow unit) domain, so comparisons are problematic, and they report only 1% accuracy in their calculations, but it is possible that they have found a periodic orbit or recurrent motion analogous to those of Fig. 7(b).

An interesting class of low-dimensional models for shear flows, including PCF, was proposed by Waleffe.[14,15,18] A major difference between our models and his is that the latter include *decoupled* streamwise velocities representing the mean flow and streak modes, and cross-stream roll components, along with a "wakelike" x-dependent streak instability.[18] These lead to coexistence of a stable laminar state and a nontrivial (periodic) attractor and allow investigation of transition. Our POD-based models employ a vectorially coupled decomposition, constraining relative roll-streak magnitudes within each mode and implying instability of the laminar state, but permitting rational inclusion of a hierarchy of freely interacting modes that respect the symmetries of the problem, and whose relative amplitudes can dynamically adjust to capture the roll-streak-mean interactions. [Our simplest model, of Sec. IV B, describes interaction between the mean $a_{00}^{(1)}$ and a "most unstable" roll-streak mode $a_{0j}^{(1)}$ whose spanwise scale depends on Reynolds number. If we continue Waleffe's reduction scheme (Sec. III C of Ref. 15), assuming that his streak and roll modes U and V maintain a fixed amplitude ratio, and neglect the streamwise varying mode W, his model collapses to ours.] In Waleffe's simplest model there is only one real mode in each group, and spanwise (or streamwise) translations are not allowed, thus excluding the possibility of heteroclinic cycles of the type that we find in Sec. IV C, and that also play a crucial role in models of the turbulent boundary layer (cf. Refs. 4 and 49). Thus, both types of models impose constraints (as any low dimensional model must), and each highlights a different aspect of the turbulence production and sustainment process.

A further comment on our vectorially coupled POD bases and the resulting instability of the laminar $\mathbf{u} = \mathbf{0}$ state in

our models is appropriate. As noted in Sec. IV B, since the empirical eigenfunctions derive from turbulent DNS data that remains far from $\mathbf{u}=\mathbf{0}$, the leading basis functions induce coupling between streamwise and spanwise velocity components that leads to an energy source term [the second term on the right-hand side of Eq. (B1)], in the *absence* of modes containing explicit streamwise variations. This is because the empirical basis functions with $k_x=0$ effectively average over the longest nonzero streamwise scales. As explained by Berkooz *et al.*[7,46] and Waleffe,[14] this constraint may be relaxed by using a representation in which streamwise and spanwise components are decoupled (at the cost of doubling the number of modes). Preliminary studies of such a decomposition indicate eventual decay to the trivial state for models lacking streamwise variations, as expected. We are currently studying both coupled and decoupled models including streamwise modes, but correct representions of the energy budgets and modal interactions would require use of eddy viscosity (Heisenberg) models; this work will appear in a future paper.

The dependence of eigenvalues and energy budgets on the aspect ratio of the DNS computational domain is also of interest: as noted in Ref. 38, short domains (such as the $L_x=4\pi$ used here) cannot accommodate the largest streamwise scales in turbulent PCF, and may "artificially" force streamwise vortical structures.

ACKNOWLEDGMENTS

APPENDIX A

It may be verified from (5)–(7) and (18) that the nontrivial group elements of D_2 act on the $\mathbf{F}^{(k)}$'s as follows:

$$
\mathcal{P}\cdot\begin{pmatrix} F_1^{(k)}(n_x,n_y;z) \\ F_2^{(k)}(n_x,n_y;z) \\ F_3^{(k)}(n_x,n_y;z) \end{pmatrix} = \begin{pmatrix} -F_1^{(k)}(-n_x,-n_y;-z) \\ -F_2^{(k)}(-n_x,-n_y;-z) \\ -F_3^{(k)}(-n_x,-n_y;-z) \end{pmatrix},
\tag{A1}
$$

$$
\mathcal{R}\cdot\begin{pmatrix} F_1^{(k)}(n_x,n_y;z) \\ F_2^{(k)}(n_x,n_y;z) \\ F_3^{(k)}(n_x,n_y;z) \end{pmatrix} = \begin{pmatrix} F_1^{(k)}(n_x,-n_y;z) \\ -F_2^{(k)}(n_x,-n_y;z) \\ F_3^{(k)}(n_x,-n_y;z) \end{pmatrix},
\tag{A2}
$$

$$
\mathcal{R}\mathcal{P}\cdot\begin{pmatrix} F_1^{(k)}(n_x,n_y;z) \\ F_2^{(k)}(n_x,n_y;z) \\ F_3^{(k)}(n_x,n_y;z) \end{pmatrix} = \begin{pmatrix} -F_1^{(k)}(-n_x,n_y;-z) \\ F_2^{(k)}(-n_x,n_y;-z) \\ -F_3^{(k)}(-n_x,n_y;-z) \end{pmatrix}.
\tag{A3}
$$

APPENDIX B

Letting $'$ denote differentiation with respect to z, the coefficients of (22) are

$$
\hat{A}^{(k,n)}_{k_x k_y} = -\frac{2\pi i k_x}{L_x}\sum_{j=1}^{3}\int_{-1}^{1} z\,\phi^{(n)}_{jk_x k_y}\phi^{(k)*}_{jk_x k_y}dz
$$

$$
-\int_{-1}^{1}\phi^{(n)}_{3k_x k_y}\phi^{(k)*}_{1k_x k_y}dz - \frac{1}{Re}\left[\left(\left(\frac{2\pi k_x}{L_x}\right)^2\right.\right.
$$

$$
\left.+\left(\frac{2\pi k_y}{L_y}\right)^2\right)\delta_{nk}+\sum_{j=1}^{3}\int_{-1}^{1}\phi^{(n)\prime}_{jk_x k_y}\phi^{(k)*\prime}_{jk_x k_y}dz\Bigg],
\tag{B1}
$$

$$
\hat{B}^{(k,m,n)}_{k_x k_y m_x m_y} = -\frac{1}{\sqrt{L_x L_y}}\sum_{j=1}^{3}\int_{-1}^{1}\left(\frac{2\pi i m_x}{L_x}\phi^{(n)}_{1,k_x-m_x,k_y-m_y}\right.
$$

$$
\times\phi^{(m)}_{jm_x m_y}+\frac{2\pi i m_y}{L_y}\phi^{(n)}_{2,k_x-m_x,k_y-m_y}\phi^{(m)}_{jm_x m_y}
$$

$$
\left.+\phi^{(n)}_{3,k_x-m_x,k_y-m_y}\phi^{(m)\prime}_{jm_x m_y}\right)\phi^{(k)*}_{jk_x k_y}dz.
\tag{B2}
$$

[1] J. L. Lumley, "The structure of inhomogeneous turbulent flows," in *Atmospheric Turbulence and Wave Propagation*, edited by A. M. Yaglom and V. I. Tatarski (Nauka, Moscow, 1967), pp. 166–178.

[2] J. L. Lumley, *Stochastic Tools in Turbulence* (Academic, New York, 1971).

[3] S. Herzog, "The large scale structure in the near wall region of a turbulent pipe flow," Ph.D. thesis, Cornell University, 1986.

[4] N. Aubry, P. Holmes, J. L. Lumley, and E. Stone, "The dynamics of coherent structures in the wall region of the wall boundary layer," J. Fluid Mech. **192**, 115 (1988).

[5] S. J. Kline, "Observed structure features in turbulent and transitional boundary layers," in *Fluid Mechanics of Internal Flow*, edited by G. Sovran (Elsevier, Amsterdam, 1967), pp. 27–68.

[6] L. Sirovich, "Turbulence and the dynamics of coherent structures, Parts I–III," Q. Appl. Math. **XLV**, 561 (1987).

[7] P. Holmes, J. L. Lumley, and G. Berkooz, *Turbulence, Coherent Structures, Dynamical Systems and Symmetry* (Cambridge University Press, Cambridge, 1996).

[8] P. G. Drazin and W. H. Reid, *Hydrodynamic Stability* (Cambridge University Press, Cambridge, 1981).

[9] O. Dauchot and F. Daviaud, "Finite amplitude perturbation and spots growth mechanism in plane Couette flow," Phys. Fluids **7**, 335 (1995).

[10] M. Nagata, "Three-dimensional finite-amplitude solutions in plane Couette flow: bifurcation from infinity," J. Fluid Mech. **217**, 519 (1990).

[11] R. M. Clever and F. H. Busse, "Three-dimensional convection in a horizontal fluid layer subjected to a constant shear," J. Fluid Mech. **234**, 511 (1992).

[12] A. Schmiegel, "Transition to turbulence in linearly stable shear flows," Dissertation, University of Marburg, 1999.

[13] J. S. Baggett and L. N. Trefethen, "Low-dimensional models of subcritical transition to turbulence," Phys. Fluids **9**, 1043 (1997).

[14] F. Waleffe, "Transition in shear flows. Nonlinear normality versus non-normal linearity," Phys. Fluids **7**, 3060 (1995).

[15] F. Waleffe, "On a self-sustaining process in shear flows," Phys. Fluids **9**, 883 (1997).

[16] O. Dauchot and N. Vioujard, "Phase space analysis of a dynamical model for the subcritical transition to turbulence in plane Couette flow," Eur. Phys. J. B **14**, 377 (2000).

[17] J. Hamilton, J. Kim, and F. Waleffe, "Regeneration mechanisms of near-wall turbulence structures," J. Fluid Mech. **287**, 317 (1995).

[18] F. Waleffe, "Hydrodynamic stability and turbulence: Beyond transients to a self-sustaining process," Stud. Appl. Math. **95**, 319 (1995).

[19] F. Waleffe, "Three-dimensional coherent states in plane shear flows," Phys. Rev. Lett. **81**, 4140 (1998).

[20] B. Eckhardt and A. Mersmann, "Transition to turbulence in a shear flow," Phys. Rev. E **60**, 509 (1999).

[21] A. Schmiegel and B. Eckhardt, "Fractal stability border in plane Couette flow," Phys. Rev. Lett. **79**, 5250 (1997).

[22] G. Kawahara and S. Kida, "Periodic motion embedded in plane Couette

turbulence: Regeneration cycle and burst," J. Fluid Mech. **449**, 291 (2001).

[23] S. Sanghi and N. Aubry, "Mode interaction models for near-wall turbulence," J. Fluid Mech. **247**, 455 (1993).

[24] B. Podvin, "On the adequacy of the ten-dimensional model for the wall layer," Phys. Fluids **13**, 210 (2001).

[25] X. Zhou and L. Sirovich, "Coherence and chaos in a model of a turbulent boundary layer," Phys. Fluids A **46**, 2855 (1992).

[26] G. Berkooz, P. Holmes, J. L. Lumley, N. Aubry, and E. Stone "Observations regarding 'Coherence and chaos in a model of a turbulent boundary layer' by X. Zhou and L. Sirovich," Phys. Fluids **6**, 1574 (1994).

[27] J. S. Lomont, *Applications of Finite Groups* (Dover, New York, 1993).

[28] C. W. Rowley, T. Colonius, and R. M. Murray, "Dynamical models for control of cavity oscillations," AIAA Pap. 2001–2126 (2001).

[29] G. Berkooz and E. S. Titi, "Galerkin projections and the proper orthogonal decomposition for equivariant equations," Phys. Lett. A **174**, 94 (1993).

[30] N. Aubry, W.-Y. Lian, and E. S. Titi, "Preserving symmetries in the proper orthogonal decomposition," SIAM J. Sci. Comput. (USA) **14**, 483 (1993).

[31] M. Dellnitz, M. Golubitsky, and M. Nicol, "Symmetry of attractors and the Karhunen-Loève decomposition," in *Trends and Perspectives in Applied Mathematics*, edited by L. Sirovich (Springer-Verlag, Berlin, 1994), pp. 73–108.

[32] N. Smaoui and D. Armbruster, "Symmetry and the Karhunen–Loève analysis," SIAM J. Sci. Comput. (USA) **18**, 1526 (1997).

[33] P. Moin and R. D. Moser, "Characteristic-eddy decomposition of turbulence in a channel," J. Fluid Mech. **200**, 471 (1989).

[34] E. Anderson, Z. Bai, C. Bischof, S. Blackford, J. Demmel, J. Dongarra, J. Du Croz, A. Greenbaum, S. Hammarling, A. McKenney, and D. Sorensen, LAPACK *User's Guide*, 3rd ed. (Society for Industrial and Applied Mathematics, Philadelphia, 1999).

[35] S. Malerud, K. J. Måløy, and W. I. Goldburg, "Measurements of turbulent velocity fluctuations in a planar Couette cell," Phys. Fluids **7**, 1949 (1995).

[36] H. Faisst and B. Eckhardt, "Transition from the Couette–Taylor system to the plane Couette system," Phys. Rev. E **61**, 7227 (2000).

[37] K. H. Bech, N. Tillmark, P. H. Alfredsson, and H. I. Andersson, "An investigation of turbulent plane Couette flow at low Reynolds numbers," J. Fluid Mech. **286**, 291 (1995).

[38] J. Komminaho, A. Lundbladh, and A. V. Johansson, "Very large structures in plane turbulent Couette flow," J. Fluid Mech. **320**, 259 (1996).

[39] N. Aubry, "A dynamical system/coherent structure approach to the fully developed turbulent wall layer," Ph.D. thesis, Cornell University, 1987.

[40] O. Dauchot and F. Daviaud, "Streamwise vortices in plane Couette flow," Phys. Fluids **7**, 901 (1995).

[41] S. Bottin, O. Dauchot, and F. Daviaud, "Intermittency in a locally forced plane Couette flow," Phys. Rev. Lett. **79**, 4377 (1997).

[42] S. Bottin, O. Dauchot, F. Daviaud, and P. Manneville, "Experimental evidence of streamwise vortices as finite amplitude solutions in transitional plane Couette flow," Phys. Fluids **10**, 2597 (1998).

[43] D. Barkley and L. S. Tuckerman, "Stability analysis of perturbed plane Couette flow," Phys. Fluids **11**, 1187 (1999).

[44] M. Golubitsky, I. Stewart, and D. G. Schaeffer, *Singularities and Groups in Bifurcation Theory, Vol. II* (Springer-Verlag, New York, 1988).

[45] J. D. Crawford and E. Knobloch, "Symmetry and symmetry-breaking bifurcations in fluid mechanics," Annu. Rev. Fluid Mech. **23**, 601 (1991).

[46] G. Berkooz, P. Holmes, and J. L. Lumley, "Intermittent dynamics in simple models of the wall layer," J. Fluid Mech. **230**, 75 (1991).

[47] B. Podvin and J. Lumley, "A low-dimensional approach for the minimal flow unit," J. Fluid Mech. **362**, 121 (1998).

[48] E. Doedel, H. B. Keller, and J. P. Kernevez, "Numerical analysis and control of bifurcation problems (I) Bifurcation in finite dimensions," Int. J. Bifurcation Chaos Appl. Sci. Eng. **1**, 493 (1991).

[49] D. Armbruster, J. Guckenheimer, and P. Holmes, "Heteroclinic cycles and modulated traveling waves in systems with O(2) symmetry," Physica D **29**, 257 (1988).

[50] J. Guckenheimer and P. Holmes, *Nonlinear Oscillations, Dynamical Systems, and Bifurcations of Vector Fields* (Springer-Verlag, New York, 1983).

[51] B. D. Coller, P. Holmes, and J. L. Lumley, "Controlling noisy heteroclinic cycles," Physica D **72**, 135 (1994).

[52] B. D. Coller, P. Holmes, and J. L. Lumley, "Interaction of adjacent bursts in the wall region," Phys. Fluids **6**, 954 (1994).

[53] B. D. Coller and P. Holmes, "Suppression of bursting," Automatica **33**, 1 (1997).